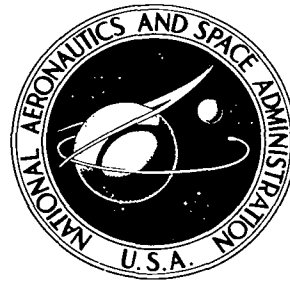


NASA TECHNICAL NOTE



NASA TN D-6689

C.1

NASA TN D-6689

LOAN COPY: RETI
AFWL (DOU
KIRTLAND AFB,

0133326



TECH LIBRARY KAFB, NM

HYPERSONIC RAREFIED FLOW OVER SHARP SLENDER CONES

*by Marvin I. Kussoy, David A. Stewart,
and Clifford C. Horstman*

*Ames Research Center
Moffett Field, Calif. 94035*





0133326

1. Report No. NASA TN D-6689	2. Government Accession No.	3. Recipient's Catalog No.	
4. Title and Subtitle HYPERSONIC RAREFIED FLOW OVER SHARP SLENDER CONES	5. Report Date March 1972		6. Performing Organization Code
	7. Author(s) Marvin I. Kussoy, David A. Stewart, and Clifford C. Horstman		8. Performing Organization Report No. A-4133
9. Performing Organization Name and Address NASA Ames Research Center Moffett Field, Calif., 94035	10. Work Unit No. 129-01-20-01-00-21		11. Contract or Grant No.
	12. Sponsoring Agency Name and Address National Aeronautics and Space Administration Washington, D. C. 20546		13. Type of Report and Period Covered Technical Note
15. Supplementary Notes		14. Sponsoring Agency Code	
16. Abstract <p>Drag, heat transfer, and number flux were measured on sharp cones in the near free molecule flow regime, and the results were compared with available Monte Carlo calculations. In general, the calculations predicted the magnitude of the data; however, the heat transfer and drag increased with increasing Knudsen number at a faster rate than predicted. Also the drag coefficients measured for the slender cones at high Knudsen number were higher than predicted for free molecule flow. These disagreements between theory and experiment could possibly be attributed to the simplicity of the surface interaction laws assumed in the theory. Reynolds analogy factors obtained from the experimental measurements agreed with free-molecule values and also with that obtained by the Monte Carlo technique.</p>			
17. Key Words (Suggested by Author(s)) Cones Rarefied flow Hypersonic flow Drag Heat transfer		18. Distribution Statement Unclassified -- Unlimited	
19. Security Classif. (of this report) Unclassified	20. Security Classif. (of this page) Unclassified	21. No. of Pages 25	22. Price* \$3.00



SYMBOLS

C_D	drag coefficient referenced to base area, $\frac{\text{mass} \times \text{acceleration}}{\frac{1}{2} \rho_{\infty} U_{\infty}^2 \frac{\pi D^2}{4}}$
\bar{C}_f	average local skin friction coefficient
C_H	Stanton number, $\frac{\dot{q}}{\rho_{\infty} U_{\infty} (H_0 - H_w)}$
D	base diameter
d	cone local diameter
H	enthalpy
l	model length
M	Mach number
m	mass per molecule
N	number flux
p	pressure
q	heat-transfer rate
R	gas constant
Re	Reynolds number
T	temperature
U	velocity
x	distance along model axis from apex
γ	ratio of specific heats
θ_c	cone semivertex angle
λ	mean free path
ρ	density

Subscripts

c	cavity (or chamber)
FM	free-molecule value
in	incident flux into cavity
o	stagnation value
or	orifice
out	out of cavity
r	reservoir
w	wall value
∞	free-stream value

HYPERSONIC RAREFIED FLOW OVER SHARP SLENDER CONES

Marvin I. Kussoy, David A. Stewart, and Clifford C. Horstman

Ames Research Center

SUMMARY

Drag, heat transfer, and number flux were measured on sharp cones in the near free molecule flow regime, and the results were compared with available Monte Carlo calculations. In general, the calculations predicted the magnitude of the data; however, the heat transfer and drag increased with increasing Knudsen number at a faster rate than predicted. Also the drag coefficients measured for the slender cones at high Knudsen number were higher than predicted for free molecule flow. These disagreements between theory and experiment could possibly be attributed to the simplicity of the surface interaction laws assumed in the theory. Reynolds analogy factors obtained from the experimental measurements agreed with free-molecule values and also with that obtained by the Monte Carlo technique.

INTRODUCTION

To date, the most promising theoretical technique for describing kinetic flow over sharp slender cones is the Monte Carlo simulation method (ref. 1). If it can be verified experimentally, this method will be a reliable way to solve many complex rarefied flow problems as well as higher Reynolds number fluid-flow problems, as advances in computer technology are made. However, there is a need for more experimental data on slender cones in the kinetic flow regime where Monte Carlo solutions are currently available. This report presents the results of a detailed experimental investigation, in which total drag, heat transfer, and surface number flux were measured on slender cones in this flow regime, and compares these results with available Monte Carlo solutions. The measurements were obtained on cones with half angles from 1.8° to 25° in air and helium at Mach numbers from 24 to 35. The Knudsen number based on cone diameter varied from 0.01 to 5.

APPARATUS AND TEST CONDITIONS

Facility and Stream Calibration

Facility— The tests were run in the Ames 42-Inch Shock Tunnel (fig. 1) with air and helium as the test gases. The tunnel has a 10° half-angle conical nozzle (2.74-m long) attached to a 15.8-cm diameter driven tube, 12.2-m long, in which a reflected shock-tailored interface reservoir of test gas is established by means of a large driver (7.66-m long and 68.6-cm diameter). For the air tests, combustion-heated helium was used in the driver, and throat diameters of 0.203 and 0.254 cm were used in the conical nozzle. The reservoir total enthalpy was 9.3 kJ/gm and total pressure was 285 atm, with Mach numbers of 24 and 27 in the hexagonal-shaped test section (1.08-m wide and

2.0-m long). For the helium tests, cold helium was used in the driver and a throat diameter of 1.535 cm was used in the conical nozzle. The reservoir total enthalpy was 2.4 kJ/gm and total pressure was 12.8 atm, resulting in a Mach number of 35 in the test section. Shock velocity and reservoir pressure were measured in the shock tube during each test.

Stream calibration— The general calibration technique used to define the stream properties of this facility is given in references 2 and 3. The stream properties for the air tests were obtained from static and impact-pressure measurements by a method (ref. 3) that assumes the sudden freeze of chemical reactions and molecular vibrations in an expanding partly dissociated test gas. The effective freeze Mach numbers were determined at upstream stations in the nozzle, since the corrections to the static pressure measurement, for thermal transpiration and boundary-layer growth were greater than 10 percent in the test section at $M_\infty = 24$ and 27. The test-section flow properties appropriate to each nozzle throat size were then obtained using the freeze Mach number determined upstream in the conical nozzle, a pitot-pressure measurement taken in the test section, and a one-dimensional nozzle expansion computer program. Probes with outside diameters from 0.5 to 4-cm were used to ensure that the test station pitot-pressure measurement was free from rarefaction effects. The measured results indicated that these effects were negligible for probe diameters greater than 1.5 cm. The run-to-run repeatability of the normalized dynamic pressure (referenced to reservoir pressure) was ± 5 percent; other stream properties as derived from computations of an expanding frozen flow of known active energy are estimated to be within ± 10 percent.

For the helium tests, the flow was assumed to act as a perfect gas in equilibrium; the stream properties were defined by the ratio of pitot pressure to reservoir pressure, and the total enthalpy. The accuracy of the stream properties, including run-to-run repeatability of normalized dynamic pressure was ± 5 percent.

The nominal test conditions for this investigation are given in table 1. For all tests, the model wall temperatures were 294° K. The mean free path was determined from the hard sphere collision model ($\lambda_\infty = 1.26 \sqrt{\gamma} M_\infty / Re_\infty / \text{cm}$). In the test section, the longitudinal Mach number gradient was less than 0.05/cm for all test conditions. Useful flow times were about 20 msec in each test gas, as determined from stream pressure and stagnation-point heat-transfer measurements, and were further verified by the drag measurements discussed.

Models

Drag— The models, cones with half angles of 1.8°, 2.5°, 5.0°, 10.0°, and 25.0°, were made by machining the forward part of the cone from a heavy material (tungsten, steel, or aluminum), gluing this tip onto a lighter material (wood or plastic), and then machining and grinding this rear part to the desired length. The model surfaces had an RMS 64 finish, and were spray-painted with a blue dye. Model lengths varied from 0.13 to 16.7 cm and the weights from 0.001 to 1.2 gm, the ratio of model weight per unit frontal area to stream pitot pressure ranged from 0.02 to 0.2 for the air tests and 0.01 to 0.1 for the helium tests.

Heat transfer— The heat-transfer models were glass cones with half-angles of 3°, 5°, 10°, and 25°, and a 2.54-cm diameter base. A typical model is shown in figure 2. Thin platinum films, approximately 10^{-5} cm thick, were painted in a concentric pattern onto a polished glass model and

then baked. A thin silicon-dioxide coating ($\sim 10^{-5}$ cm thick) was then vacuum deposited onto the model. The gage construction technique and materials used were the same as reported in reference 4. The surface finish on these glass models was \sim RMS 128.

Number flux— The number-flux models were stainless-steel cones with half-angles of 3° and 5° and base diameters of 2.54 cm. They were constructed in sections and assembled to provide number-flux measurements at several positions along the surface. The large cavity in the conical sections (see fig. 3) had a small sharp-lipped orifice at the surface with a lip thickness less than 0.007 cm. A variable capacitance, diaphragm-type, pressure cell was installed in the cavity, as illustrated schematically in figure 3, and a thermocouple junction was located just behind the cavity wall. The surface finish of these models was \sim RMS 64.

MEASURING TECHNIQUE AND DATA REDUCTION

Drag Tests

Drag obtained was measured by a free-flight technique similar to that described by Geiger in reference 5. Figure 4 is a sketch of the launch setup. Several cone models were placed on cradles attached to an explosively driven retractable table; the models were spaced 3-cm or two model lengths apart, whichever distance was greater. Prior to a run, the models were outgassed for 3 hours at less than 10μ Hg. The table was retracted 2 msec before the start of flow to a position 16-cm below its original location on the tunnel centerline (fig. 4). No model motion could be detected when the table was withdrawn. With the models motionless in the test section, the nozzle flow started and high-speed cameras recorded the flight in both the pitch and yaw planes. The model traveled from 1 to 10 cm during the 20 msec run time depending on the conditions and model configuration. Models were selected so that all those of a particular run traveled approximately the same distance. On occasion, a model would pitch or yaw when flow started. Data were discarded when the cones pitched (or yawed) to an average angle of attack greater than 4° , or greater than the cone semivertex angle, whichever was less.

A small sphere (0.5-cm diam) of known drag coefficient was also placed on the table to obtain the test-section dynamic pressure during each run. The drag coefficient of this sphere, measured by the method outlined below, had been determined earlier for each nominal test condition by simultaneously free-flying the sphere and measuring pitot pressure. In all cases, the normalized dynamic pressure determined from the sphere was within 8 percent of the computed nominal test values. The pitot-probe measurements were more accurate (± 5 percent) as mentioned previously. However, the sphere was used instead of a pitot probe with its associated sting to minimize test-section flow disturbances.

The cone-drag coefficient was the product of model mass and acceleration divided by the tunnel dynamic pressure, and referenced to the cone base area. The model acceleration was assumed constant and obtained from the slope of a straight line fitted to the measured model displacement versus time-squared curve. The displacement measurements were obtained from enlarged prints of the film record. The data, when plotted in this manner, fell in a straight line for about 20 msec, demonstrating the lack of any initial impulse to the models upon launch. Since the film rate was

500 frames/sec, zero time (flow start) could be in error by as much as 1 msec. Because of this error, and the uncertainties in the dynamic pressure, the accuracy of the drag data has been estimated to be ± 10 percent.

Heat-Transfer Tests

The heat-transfer data were obtained by measuring the surface temperature rise as indicated by the resistance change of the platinum film and processing the signal through an electrical analog circuit (see ref. 6) in which analog output is proportional to heat-transfer rate. The physical constants of the gage backing material (Pyrex 7740) were obtained by the calibration method described in reference 7. (The gage constants obtained for the 5° half-angle cone were not consistent with those for the other models used in these tests or those given in reference 7. Therefore, the heat-transfer results are not reported for this cone.) In the analysis of this type of gage the heat transfer to the model is assumed to be equivalent to that into a backing material of infinite thickness. This assumption was verified for the present test conditions by the radial temperature distribution computed as a function of time, using the heat-conduction solutions for a solid cylinder with a constant film coefficient (ref. 8). For all test conditions, the local cone diameter was larger than that required for semi-infinite heat conduction for 20 msec. The accuracy of these data was estimated to be ± 20 percent.

Number-Flux Tests

To obtain incident number flux, a technique originally proposed by Patterson and developed by Horstman (refs. 9 and 10, respectively) was used in which a pressure free of large orifice correction is measured in a large cavity with a small, sharp-lipped orifice, as described earlier. The cavity design allows the incoming high-energy molecules enough collisions with the cavity wall to accommodate to the wall temperature. For these tests, the cavity wall temperature stayed constant at 294° K. If the mean free path of the gas in the cavity, λ_c , is much larger than the orifice diameter, the outgoing number flux from the cavity is given by $N_{\text{out}} = (p_c/m)/(\sqrt{2\pi RT_c})$, where T_c and p_c denote the measured quantities in the cavity. This is the expression for free-molecular flow through an orifice for molecules with a Maxwellian energy distribution. Horstman has shown (ref. 10) that λ_c could be as small as the orifice diameter with no change in the measured results. Furthermore, the analysis assumes that for steady state, the incoming and outgoing number fluxes are equal, and incoming and outgoing molecules do not collide at the orifice. (This assumption is reasonable since both molecular streams have large mean free paths in the vicinity of the orifice.) A stretched-diaphragm, variable-capacitance pressure cell was used to measure the cavity pressure. This cell, and its calibration procedures, are described in references 11 and 12. The measured pressure is directly proportional to a capacitance change (diaphragm reflection) of the cell, which is part of a bridge circuit modulated by a 100-kc sinusoidal signal. The particular cells used in the number-flux measurements had a full-scale rating of $100 \mu\text{Hg}$, a sensitivity of 3.3×10^{-4} pF/ μHG , and a natural frequency of 10^4 Hz. The error due to sting acceleration effects was less than ± 5 percent. Thermal effects on the cell were negligible, because of the cavity design.

Number-flux data were obtained only for 3° and 5° cones in air. For both cones, λ_c varied from 1.3 to 4.5 times the orifice diameter. Data could not be obtained for the larger cone angles or in helium because the measured cavity pressures were too high to meet the requirements for

free-molecular effusive flow through the orifice. The criterion used to determine steady-state conditions in the cavity was based on the ratio of p_c/p_T being constant with time. Data not conforming were discarded. The accuracy of these data was estimated to be ± 20 percent.

RESULTS AND DISCUSSION

Cone Drag

The drag results in air and helium are given in table 2 and in figure 5 in the form C_D vs. λ_∞/D for $\theta_c = 1.8^\circ, 2.5^\circ, 5^\circ, 10^\circ,$ and 25° . The data are plotted in this particular manner since the Monte Carlo solutions are independent of cone angle when presented in this way. For reference, the free-molecule limits of C_D , computed assuming diffuse reflection and unit thermal accommodation, are also shown. At high λ_∞/D , the drag coefficient for the 2.5° cone is significantly higher than the free-molecule value ($C_D = 3$ at $\lambda_\infty/D = 4$). A similar trend was evident from the limited results of the 1.8° cone. In contrast, the 10° and 25° cone data appear to approach their respective free-molecule limits. Slender-cone drag above free molecule values has been obtained theoretically (refs. 13 and 14), but never to the magnitude shown here. Sims (ref. 15) experimentally obtained C_D on slender cones at low Mach numbers which were somewhat above those for free molecule flow. However, as far as can be determined, this is the first time these high values of C_D have been experimentally observed for cones in hypersonic flow. Over the range of λ_∞/D , where both air and helium data were obtained, there is agreement, within the experimental accuracy, between the hot-wall helium and cold-wall air results: the reason for this is not presently known. Previous drag data (refs. 5 and 16) agree with the present results.

Available Monte Carlo calculations¹ for hard sphere molecules, based on diffuse reflection and complete energy accommodation are also shown in figure 5. When plotted in the present form, C_D vs. λ_∞/D , all computed points for $\theta_c = 3^\circ, 6^\circ, 8^\circ,$ and 10° fall within the indicated statistical scatter bar. The trend of the data indicate a higher slope than that indicated by theory. There is agreement between these calculations and both air and helium data for $\lambda_\infty/D < 10^1$; however, the calculations underpredict the air data for $\lambda_\infty/D > 10^1$. At high λ_∞/D the difference between theory and experiment could be due either to differences in the diatomic molecule collision process and the hard sphere model used by the theory, or to the assumed form of the surface reflection and energy accommodation laws. At the high-energy conditions present in these tests, the intermolecular potential is nearly vertical, and molecular collisions are well approximated by the hard-sphere model. Thus the difference between theory and experiment is perhaps due to the surface interaction laws. This may explain the agreement between the calculations and the data at low Knudsen numbers, since surface interaction laws should diminish in importance with decreasing Knudsen number. Although many surface interaction laws have been proposed (e.g., ref. 17), there are presently no Monte Carlo calculations for cones that do not use the diffuse reflection and complete energy accommodation laws mentioned previously.

Skin Friction

Average local skin friction coefficients (\bar{C}_f) were deduced from the air drag results by the method discussed in reference 16. For the present results, the estimated pressure drag (using the

¹Reference 1 and a private communication from F. W. Vogenitz in January 1970.

cone pressure correlations developed in ref. 18) was less than 5 percent of the total drag for the slender cones. For the 25° half-angle cone, rough estimates of the pressure drag were a significant portion of the total drag (up to 50 percent). Therefore C_f was not computed for these cones. For the $\theta_c = 1.8^\circ$ cones \bar{C}_f is not shown, since the Knudsen number range covered for these cones was limited. For any given cone half angle, there was no discernible difference between the deduced \bar{C}_f results for the two test conditions ($M_\infty = 24$ and 27 in air). The accuracy of the deduced skin-friction data for the slender cones was estimated to be ± 12 percent. Specific values of \bar{C}_f are given in table 3, mean lines of \bar{C}_f , normalized by free-molecular values, are plotted in figure 6 vs. λ_∞/D . These results are consistent with the drag results.

Heat Transfer

The heat-transfer results, normalized by free-molecule values (computed for unit thermal and momentum accommodation) are given in table 4 and plotted vs. Knudsen number based on local diameter (λ_∞/d) in figure 7. These data were obtained in air for $\theta_c = 3^\circ, 10^\circ$, and 25° . (Helium results were not obtained since the tunnel conditions were not sufficiently rarefied.) For $\lambda_\infty/d < 0.8$, there is general agreement between the 3° and 10° data. At low λ_∞/d , the 25° data are higher than those for the more slender cones, since 25° data are approaching a higher continuum limit. The heat-transfer results of figure 7 cannot be compared directly with the drag results (fig. 5) since one is an integrated effect over a cone of diameter D , while the other is a point measurement at a local diameter, d .

The Monte Carlo calculations (refs. 1, 17) are also shown on this figure. The computed points for θ_c of $3^\circ, 6^\circ, 8^\circ$, and 10° fall within the indicated scatter band. Even though the trend of the slender-cone heat-transfer data indicate a greater slope than the calculations, most of the data for $\lambda/d > 0.2$ agree fairly well with the calculations. Again it can be speculated that different accommodation and reflection laws would perhaps alter the Monte Carlo calculations and improve the agreement with these data.

Number Flux

Number-flux data, normalized by the free-molecule flux, are given in table 5, and in figure 8 are plotted vs. Knudsen number based on local diameter (λ_∞/d) for 3° and 5° cones in air. Over the entire range of λ_∞/d , there is no discernible difference (within the ± 20 percent accuracy quoted previously) between the results obtained from the 3° and 5° cones. The available Monte Carlo calculations for $3^\circ, 6^\circ$, and 8° cones are also shown on this figure. (There are presently no predictions for the flux on more slender cones for $\lambda_\infty/d < 0.2$). As with the drag and heat-transfer predictions, the number flux for the $3^\circ, 6^\circ$, and 8° cones does not differ within the statistical scatter indicated. Since these flux measurements and predictions are not directly dependent on surface interactions, the good comparison between theory and experiment at high Knudsen number indicates the validity of the Monte Carlo simulation technique.

Reynolds Analogy

The Reynolds analogy factor, $\bar{C}_f/2C_H$ (the inverse of that used in continuum flow) can be obtained directly from the present skin-friction and heat-transfer results. For each value of λ_∞/d at which heat transfer was measured $\bar{C}_f/2C_H$ was computed. (In the computations for the 3° cone \bar{C}_f was assumed to be the same as for the 2.5° cone.) The $\bar{C}_f/2C_H$ results are presented in table 6 and in figure 9. (Two points at $\lambda_\infty/d \approx 0.1$ for the 3° cone were not plotted, since they were 40 to 70 percent above the average of the other data points, probably reflecting inaccuracies in the heat-transfer measurements. These points are, however, included in the table.) The Reynolds analogy factor varies from about 0.8 to 1.30. Most of the points fall between 1.0 and 1.2, with the average of all points at 1.09. These values agree with the free molecule value ($1.166 \cos \theta_c$) if tangential and thermal accommodation coefficients are assumed equal to 1.0 (or to each other). The simple free-molecule relationship between skin friction and heat transfer on sharp slender cones could be used therefore with some confidence in the near-free-molecule regime; this result was also found by Vogenitz in reference 1.

CONCLUDING REMARKS

Drag, heat transfer, and number flux were measured on sharp cones in the near-free-molecule flow regime, and the results were compared with available Monte Carlo calculations for hard-sphere molecules. High drag coefficients, some considerably above accepted free molecule values, were measured for slender cones at high Knudsen numbers; the Monte Carlo technique did not predict these measurements. In addition, the drag and heat-transfer data increased with Knudsen number at a faster rate than that predicted by theory. This disagreement between experiment and theory may be due to either the nature of the surface interaction laws or the molecular collision model used in the theory. Reynolds analogy factors of 1.1 were obtained for the 3° and 10° cones from the measured heat-transfer data and a local skin-friction coefficient deduced from the drag data. These results agree with the free-molecule values, and the near-free-molecular results obtained by Vogenitz. It must be recognized, however, that although the experimental data have demonstrated the basic validity of the Monte Carlo simulation method to describe kinetic flow over sharp slender cones, further experimental and theoretical work are needed to resolve the discrepancies between them.

Ames Research Center
National Aeronautics and Space Administration
Moffett Field, Calif., 94035, Oct. 7, 1971

REFERENCES

1. Vogenitz, F. W.; and Takata, G. Y.: Rarefied Hypersonic Flow About Cones and Flat Plates by Monte Carlo Simulation. AIAA J., vol. 9, no. 1, Jan. 1971, pp. 94-100.
2. Loubisky, William J.; Hiers, Robert S.; and Stewart, David A.: Performance of a Combustion Driven Shock Tunnel With Application to the Tailored-Interface Operating Conditions. Proc. Third Conference on Performance of High Temperature Systems, Dec. 7-9, 1964.
3. Hiers, Robert S., Jr.; and Reller, John O., Jr.: Analysis of Nonequilibrium Air Streams in the Ames 1-Foot Shock Tunnel. NASA TN D-4985, 1969.
4. Vidal, R. J.: Model Instrumentation Techniques for Heat Transfer and Force Measurements in a Hypersonic Shock Tunnel. WADC TN-56-315, Cornell Aeronautical Lab., Buffalo, N. Y., Feb. 1956.
5. Geiger, R. E.: Slender Cone, Zero Angle of Attack Drag in Continuum and Non-Continuum Flow. Paper 69-711, AIAA, June 1969.
6. Skinner, G. T.: Analog Network to Convert Surface Temperature to Heat Flux. ARS J., vol. 30, no. 6, June 1960, pp. 569-570.
7. Skinner, G. T.: Calibration of Thin Film Gage Backing Materials. ARS J., vol. 31, no. 5, May 1961, pp. 671-672.
8. Schneider, Paul J.: Conduction Heat Transfer. Addison-Wesley Publishing Co., Reading, Mass., 1957, Ch. 10, p. 229.
9. Patterson, Gordon N.: Theory of Free-Molecule, Orifice-Type Pressure Probes in Isentropic and Nonisentropic Flows, UTIA Rep. 41 (Revised), Inst. Aerophys., Univ. Toronto, April 1959.
10. Horstman, Clifford C.: Number Flux Measurements on Sharp Plates and Wedges in the Kinetic Flow Regime. Presented at the Seventh International Symposium on Rarefied Gas Dynamics, Pisa, Italy, June 1970.
11. Dimeff, John: A Survey of New Developments in Pressure Measuring Techniques in NACA. AGARD Conference, London, March 24-28, 1958.
12. Bowman, Gary H.; and Coon, Grant W.: Static Pressure Measurements in a Hypervelocity Shock Tunnel. AIAA J., vol. 3, no. 4, April 1965, pp. 751-752.
13. Ortloff, C. R.: Hypersonic Low Density Transitional Regime Flow Over Conical Vehicles. Rep. GRC TM 805, General Research Corp., Santa Barbara, Calif., 1968.
14. Keel, A. G., Jr.; and Willis, D. R.: Critique of Near-Free Molecule Theories for Flow Over Cones. Rep. No. AS-71-5, Univ. of Calif., Berkeley, College of Eng., July 1971.

15. Sims, William H.: Drag Coefficients of Sharp and Blunt Cones in Highly Rarefied, Supersonic Flow. Rarefied Gas Dynamics. Supplement 5, Vol. I, Academic Press, N. Y., 1969, pp. 575-581.
16. Kussoy, Marvin I.; and Horstman, Clifford, C.: Cone Drag in Rarefied Hypersonic Flow. AIAA J., vol. 8, no. 2, Feb. 1970, pp. 315-320.
17. Hurlbut, F. C.; and Sherman, F. S.: Application of the Nocilla Wall Reflection Model to Free-Molecule Kinetic Theory. Phys. Fluids, vol. 11, no. 3, March 1968, pp. 486-496.
18. Kussoy, Marvin I.; and Horstman, Clifford C.: An Experimental Study of Hypersonic Rarefied Flow Over Sharp Cones. Rarefied Gas Dynamics. Supplement 5, Vol. I, Academic Press, N. Y., 1969, p. 607.

TABLE 1.-- NOMINAL STREAM CONDITIONS FOR THE 42-INCH SHOCK TUNNEL

γ	Gas	M_∞	Re_∞/cm	T_w/T_o	λ_∞, cm	H, kJ/gm	p_r, atm
1.4	Air	27.2	221	0.035	0.183	9.3	285
1.4	Air	24.5	236	.035	.155	9.3	285
1.67	Helium	34.6	5354	.68	.011	2.4	12.8

TABLE 2.- DRAG COEFFICIENT RESULTS

AIR $M_\infty = 27.2$, $Re_\infty/cm = 221$, $\lambda_\infty = 0.183$ cm, $T_w/T_\infty = 5.3$, $T_w/T_0 = 0.035$, $T_w = 294^\circ$ K				AIR $M_\infty = 24.5$, $Re_\infty/cm = 236$, $\lambda_\infty = 0.155$ cm, $T_w/T_\infty = 4.1$, $T_w/T_0 = 0.035$, $T_w = 294^\circ$ K				HELIUM $M_\infty = 34.6$, $Re_\infty/cm = 5354$, $\lambda_\infty = 0.011$ cm, $T_w/T_\infty = 272$, $T_w/T_0 = 0.68$, $T_w = 294^\circ$ K								
θ_c , deg	l , cm	C_D	$C_{D, FM}$	θ_c , deg	l , cm	C_D	$C_{D, FM}$	θ_c , deg	l , cm	C_D	$C_{D, FM}$					
1.8	2.54	2.34,2.52	2.17	1.8	2.54	2.37	2.22	1.8	2.54	0.99,1.04,1.06	2.08					
	5.08	2.07,2.26										5.08	2.15,2.18	5.08	0.67,0.95	
2.5	0.51	2.62,2.67,2.80,2.82	2.06	2.5	0.97	2.40,2.48,2.64	2.09	2.5	0.51	1.23,1.43,1.73	2.05					
		2.84,2.87,3.01,3.05			1.27	2.21			0.97	1.00,1.05,1.24,1.32						
	0.97	2.24,2.26,2.46,2.50,2.72			2.54	2.01,2.24			1.27	1.03,1.21,1.26						
	2.54	1.85,1.96,2.06			5.08	1.72,1.78			2.54	0.91						
	5.08	1.88,1.89			10.16	1.30,1.42			5.08	0.50,0.54,0.62						
5.0	0.25	2.15,2.30	2.02	5.0	0.51	2.19,2.32	2.02	5.0	0.25	1.29	2.08					
	0.51	2.08,2.12,2.38			0.97	1.94			0.51	1.00,1.15,1.19						
	0.97	1.82,2.01,2.06,2.06,2.07			1.27	2.00,2.12,2.16			0.97	0.91,0.92,0.97						
	2.54	1.79			2.54	1.64			1.27	0.67,0.83,0.90						
					5.08	1.28,1.49			2.54	0.68						
10.0	0.20	1.94	2.03	10.0	0.19	2.19	2.03	10.0	0.51	0.85,0.86	2.15					
	0.25	2.04,2.04,2.13			0.25	1.97			0.64	0.77						
	0.51	1.82,2.01			0.51	1.90			1.27	0.54,0.58						
	0.64	2.06			1.33	1.49			2.54	0.35,0.37,0.38,0.46						
	1.27	1.75			2.54	1.31,1.43										
	2.54	1.43,1.59			5.08	0.94,0.99										
	25.0	0.13			1.98,2.05,2.20,2.24	2.08			25.0	0.13		2.03,2.19,2.22	2.08	25.0	0.20	0.85,1.10,1.18
		0.20			2.11,2.21					0.19		2.34			0.25	0.88
	0.25	2.14,2.20	0.25	1.96	0.32		0.71,0.81									
	0.32	2.23	0.32	2.02	0.64		0.62,0.74									
	1.27	1.52	0.64	1.96	1.27		0.43,0.53									
			1.27	1.57,1.29												
			2.54	1.29,1.43												

TABLE 3.- SKIN-FRICTION COEFFICIENT RESULTS

AIR $M_\infty = 27.2$, $Re_\infty/cm = 221$, $\lambda_\infty = 0.183$ cm, $T_w/T_\infty = 5.3$, $T_w/T_0 = 0.035$, $T_w = 294^\circ$ K				AIR $M_\infty = 24.5$, $Re_\infty/cm = 236$, $\lambda_\infty = 0.155$ cm, $T_w/T_\infty = 4.1$, $T_w/T_0 = 0.035$, $T_w = 294^\circ$ K			
θ_c , deg	x, cm	$\bar{C}_f/C_{f,FM}$	$C_{f,FM}$	θ_c , deg	x, cm	$\bar{C}_f/C_{f,FM}$	$C_{f,FM}$
2.5	0.33	1.38	0.089	2.5	0.64	1.19	0.091
	0.81	1.20			1.17	1.01	
	2.01	0.97			2.11	0.90	
	4.24	0.79			4.24	0.70	
5.0	0.18	1.13	0.174	5.0	8.46	0.58	0.174
	0.43	1.07			0.33	1.07	
	0.81	0.99			0.81	0.96	
	2.01	0.82			1.17	0.89	
10.0	0.13	1.01	0.342	10.0	2.11	0.75	0.342
	0.23	1.00			4.24	0.53	
	0.43	0.95			0.13	1.01	
	0.58	0.88			0.23	1.00	
	1.07	0.78			0.43	0.92	
	2.11	0.62			1.07	0.76	
					2.13	0.60	
					4.24	0.41	

TABLE 4.- SURFACE HEAT-TRANSFER RESULTS

AIR $M_\infty = 27.2$, $Re_\infty/cm = 221$, $\lambda_\infty = 0.183$ cm, $T_w/T_\infty = 5.3$, $T_w/T_0 = 0.035$, $T_w = 294^\circ$ K				AIR $M_\infty = 24.5$, $Re_\infty/cm = 236$, $\lambda_\infty = 0.155$ cm, $T_w/T_\infty = 4.1$, $T_w/T_0 = 0.035$, $T_w = 294^\circ$ K			
θ_c , deg	x, cm	\dot{q}/\dot{q}_{FM}	\dot{q}_{FM} , W/cm ²	θ_c , deg	x, cm	\dot{q}/\dot{q}_{FM}	\dot{q}_{FM} , W/cm ²
3.0	1.02	0.77,0.94	3.608	3.0	1.02	0.82	4.850
	1.07	0.87			1.22	0.94	
	1.22	1.02,1.05			2.08	0.73	
	2.08	0.84			3.66	0.59	
	3.66	0.59,0.60			5.44	0.53	
	5.44	0.54			9.14	0.54	
	9.14	0.50,0.51			13.97	0.22	
	13.06	0.33			16.76	0.19	
	13.94	0.22,0.36					
	16.74	0.30					
10.0	21.60	0.15	12.480	10.0	0.91	0.58	17.220
	0.91	0.59			1.12	0.62	
	1.12	0.72			1.62	0.45	
	1.63	0.50			2.39	0.37	
	2.39	0.51			3.71	0.29	
	3.71	0.31			5.44	0.25	
25.0	5.44	0.25	30.370	25.0	0.08	0.74	41.900
	0.08	0.69			0.30	0.59	
	0.30	0.62			0.46	0.74	
	0.46	0.66			0.74	0.68	
	0.74	0.60			1.12	0.56	
	0.91	0.53			1.57	0.49	
	1.12	0.50			2.11	0.41	
	1.57	0.32					
2.11	0.43						

TABLE 5 - SURFACE NUMBER-FLUX RESULTS

AIR $M_\infty = 27.2$, $Re_\infty/cm = 221$, $\lambda_\infty = 0.183$ cm, $T_w/T_\infty = 5.3$, $T_w/T_0 = 0.035$, $T_w = 294^\circ$ K				AIR $M_\infty = 24.5$, $Re_\infty/cm = 236$, $\lambda_\infty = 0.155$ cm, $T_w/T_\infty = 4.1$, $T_w/T_0 = 0.035$, $T_w = 294^\circ$ K			
θ_c , deg	x, cm	N/N _{FM}	N _{FM} , molecules/cm ² sec	θ_c , deg	x, cm	N/N _{FM}	N _{FM} , molecules/cm ² sec
3.0	3.18	0.96	0.852×10^{19}	3.0	3.18	1.00	1.145×10^{19}
	3.51	0.87			3.51	0.73,0.87	
	4.95	1.23			4.95	1.14	
	8.79	0.76			8.79	0.70,0.86	
	12.07	0.81,0.87,0.89,0.96			12.07	0.67,0.73,0.77, 0.88,0.94,0.95	
5.0	2.41	0.88	1.481×10^{19}	5.0	2.41	0.76,0.95	2.020×10^{19}
	4.95	0.91			7.11	0.82,0.91	
	6.68	0.97			8.71	0.73	
	7.11	0.89			12.09	0.51,0.61,0.62	
	12.09	0.67,0.86					

TABLE 6.- REYNOLDS ANALOGY RESULTS

AIR $M_\infty = 27.2$, $Re_\infty/cm = 221$, $\lambda_\infty = 0.183$ cm, $T_w/T_\infty = 5.3$, $T_w/T_0 = 0.035$, $T_w = 294^\circ$ K				AIR $M_\infty = 24.5$, $Re_\infty/cm = 236$, $\lambda_\infty = 0.155$ cm, $T_w/T_\infty = 4.1$, $T_w/T_0 = 0.035$, $T_w = 294^\circ$ K			
θ_c , deg	x, cm	$\bar{C}_f/2C_H$	$(\bar{C}_f/2C_H)_{FM}$	θ_c , deg	x, cm	$\bar{C}_f/2C_H$	$(\bar{C}_f/2C_H)_{FM}$
3°	1.02	1.086,1.342	1.166	3°	1.02	1.190	1.166
	1.07	1.205			1.22	1.000	
	1.22	0.951,0.974			2.08	1.124	
	2.08	1.039			3.66	1.152	
	3.66	1.197,1.240			5.44	1.103	
	5.44	1.200			9.14	0.824	
	9.14	0.966,0.986			13.97	1.510 ^a	
	13.06	1.204					
	13.94	1.074,1.726 ^a					
	16.74	1.096					
10°	0.91	1.051	1.150	10°	0.91	1.056	1.150
	1.12	0.830			1.12	0.907	
	1.63	1.086			1.62	1.127	
	2.39	0.947			2.39	1.154	
	3.71	1.173			3.71	1.184	
	5.44	1.255					

^aNot plotted.

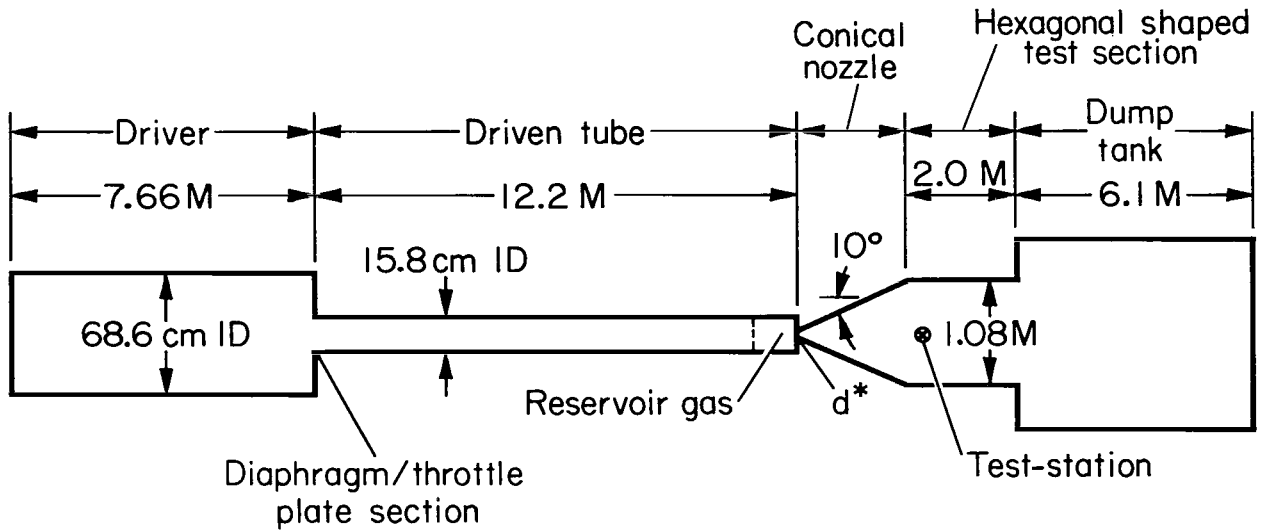


Figure 1.- Sketch of Ames 42-Inch Shock Tunnel.

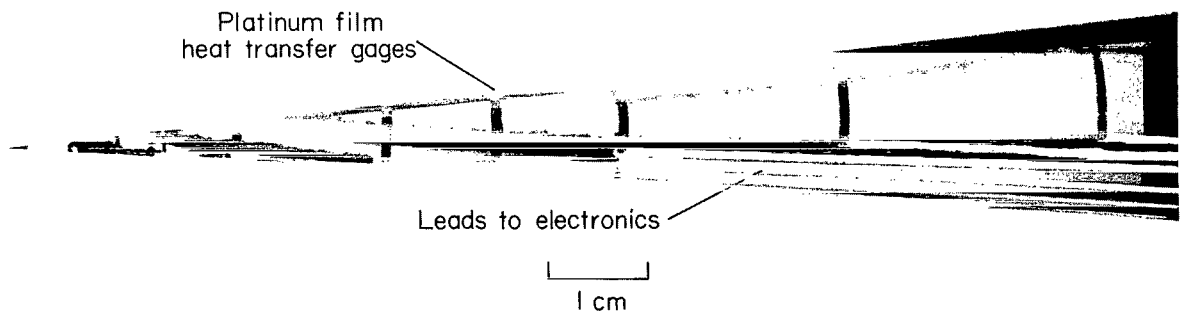
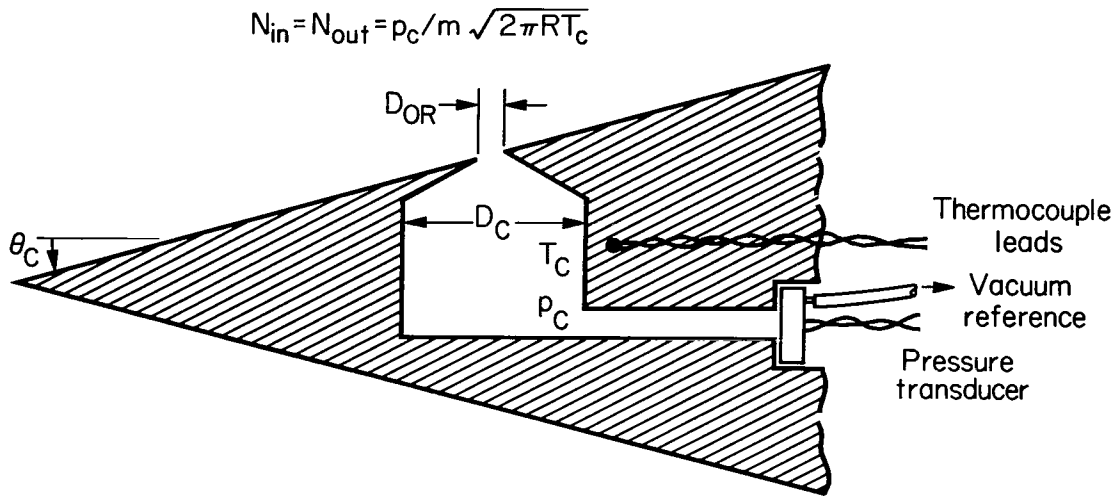


Figure 2.- Typical heat-transfer model.



θ_C , deg	D_{OR} , cm	D_C , cm
3	0.085	0.2 - 0.3
5	0.050	0.15 - 0.3

Figure 3.- Typical number-flux cavity and orifice.

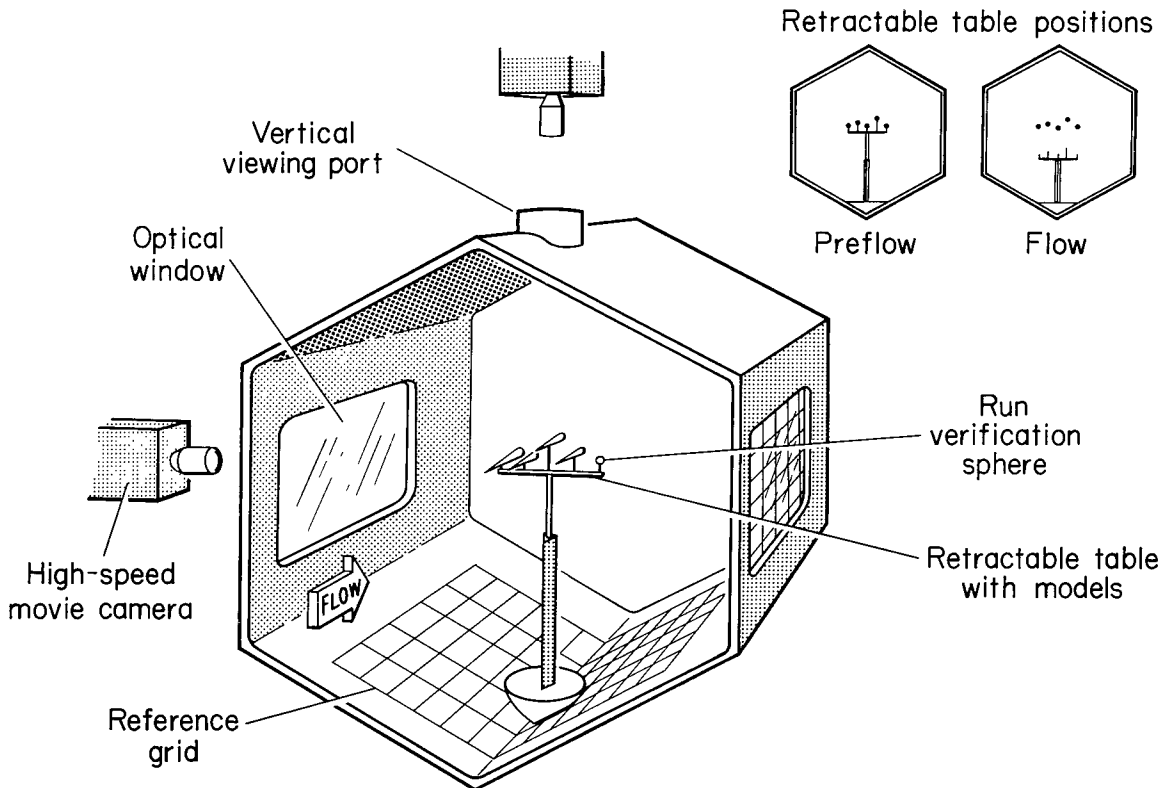


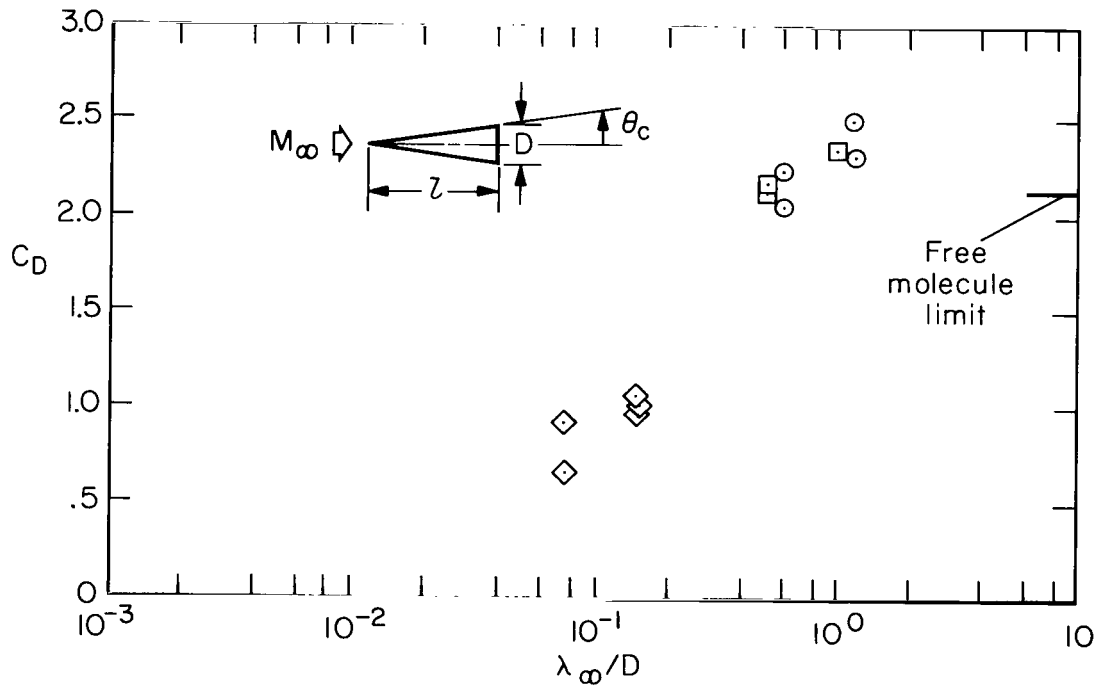
Figure 4.- Free-flight test setup in shock tunnel.

θ_c					γ	Gas	M_∞	$\lambda_\infty, \text{cm}$	T_w/T_0
1.8°	2.5°	5°	10°	25°					
○	○	○	○	○	1.4	Air	27.2	0.183	0.035
□	□	□	□	□	1.4	Air	24.5	.155	.035
	△	△	△	△	1.4	Air	15-25	0.023-0.155	.035 (Ref. 16)
◇	◇	◇	◇	◇	1.67	Helium	34.6	.011	.68

$\times \theta_c = 6^\circ$ $\gamma = 1.4^\circ$, $M_\infty = 22-24$, $T_w/T_0 = 0.11-0.13$ (Ref. 5)

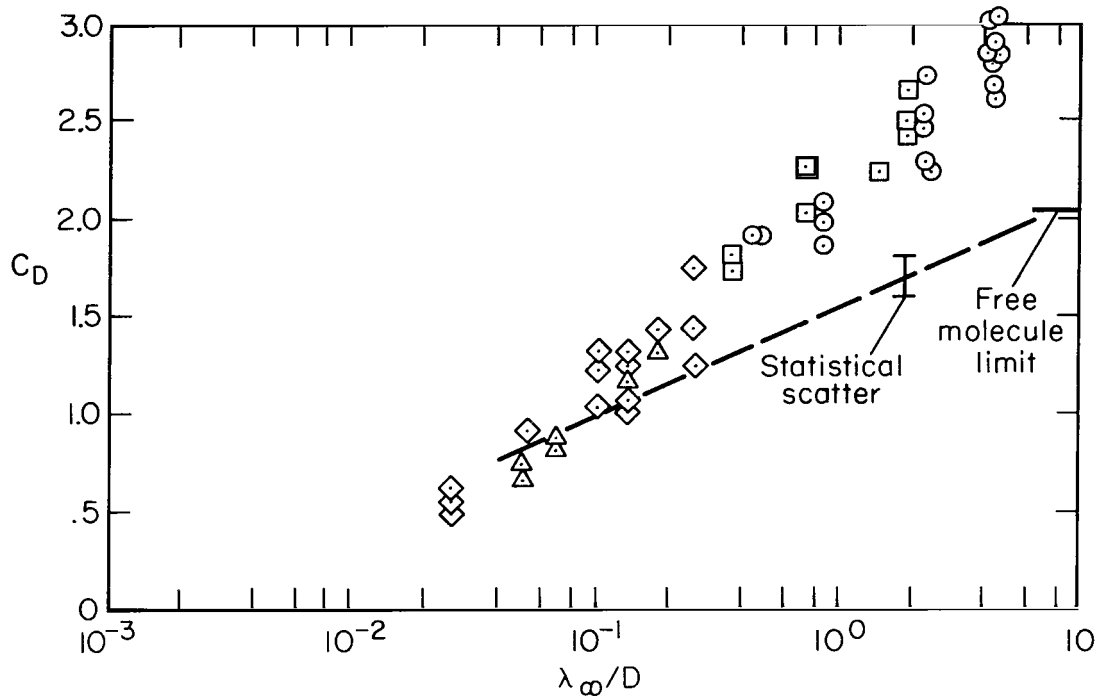
- Monte-Carlo calculations (Ref. 1)
hard-sphere molecules
 $\theta_c = 3^\circ$ to 10° , $M_\infty = 24$, $T_w/T_0 = 0.01-0.13$
- Monte-Carlo calculations (F. W. Vogenitz, Private Communication, Jan 1970)
hard-sphere molecules
 $\theta_c = 5^\circ$, $M_\infty = 24$, $T_w/T_0 = 0.72$

(a) Key.

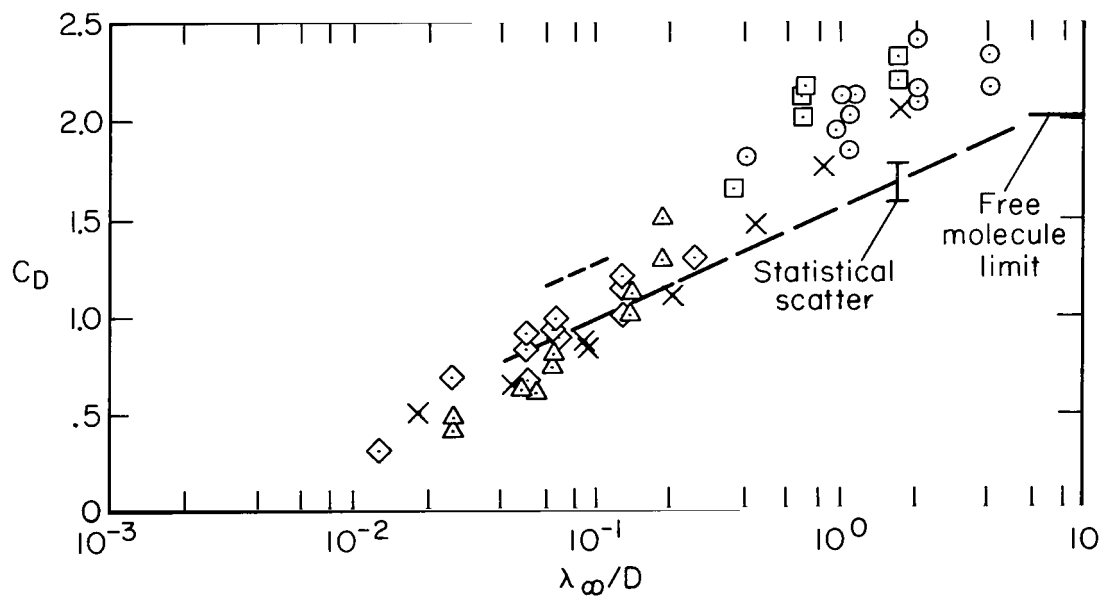


(b) $\theta_c = 1.8^\circ$

Figure 5.- Variation of cone-drag coefficient with Knudsen number.

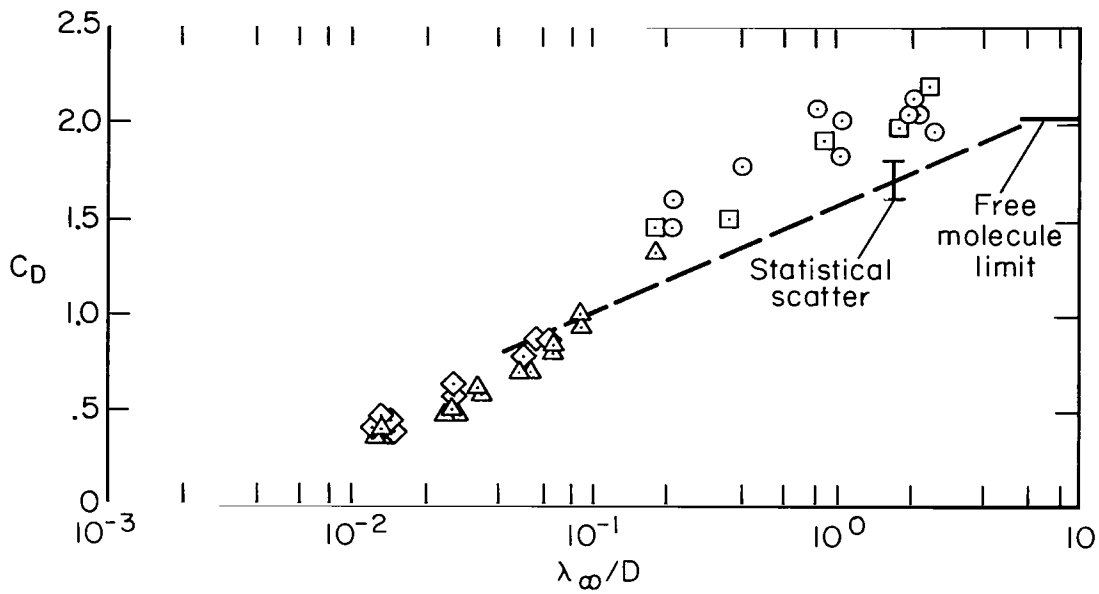


(c) $\theta_c = 2.5^\circ$

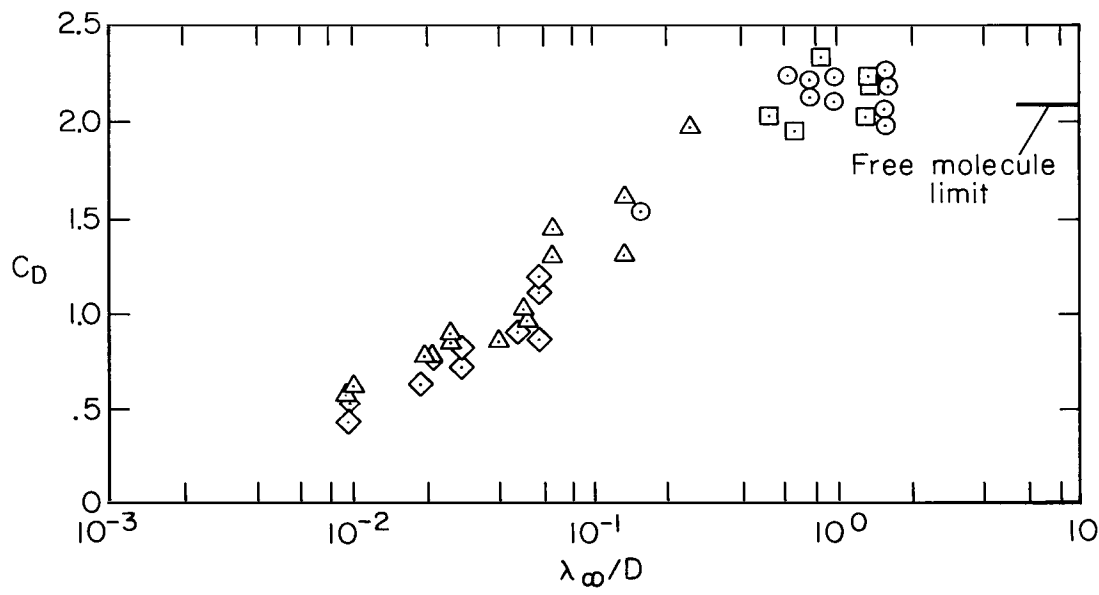


(d) $\theta_c = 5.0^\circ$

Figure 5.- Continued.



(e) $\theta_c = 10^\circ$



(f) $\theta_c = 25^\circ$

Figure 5.- Concluded.

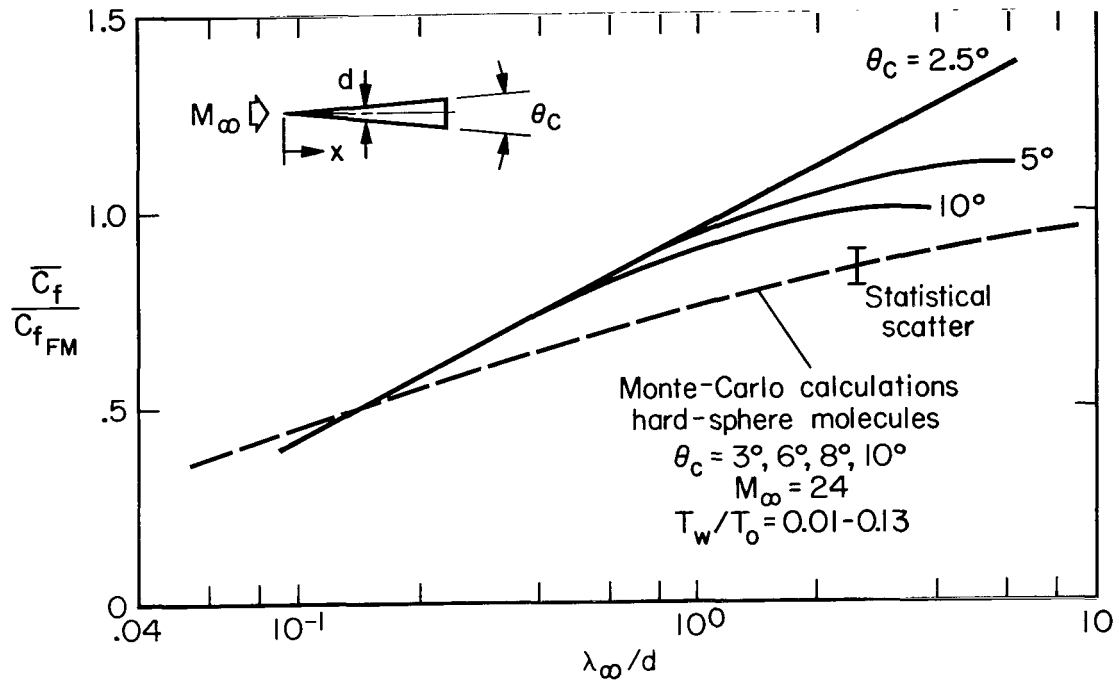
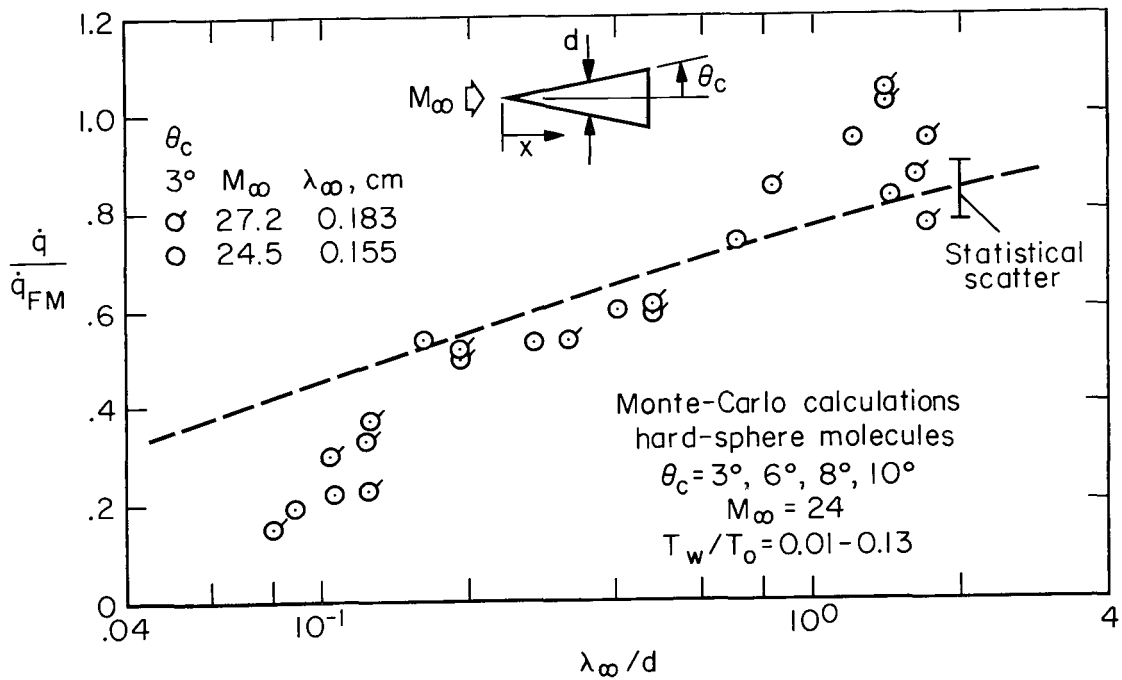
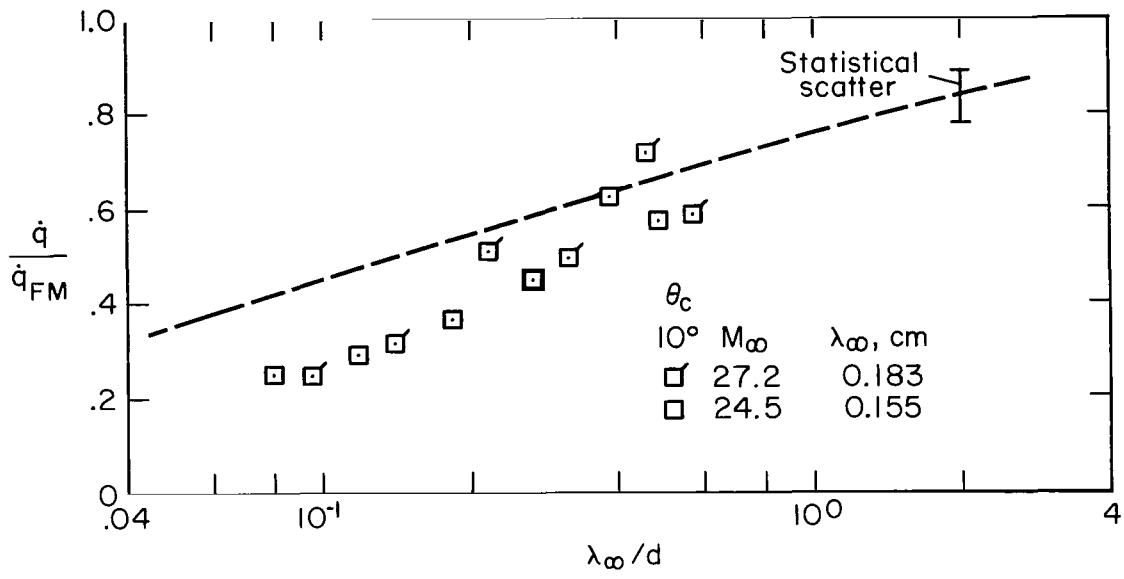


Figure 6.- Normalized skin-friction coefficient variation with Knudsen number.

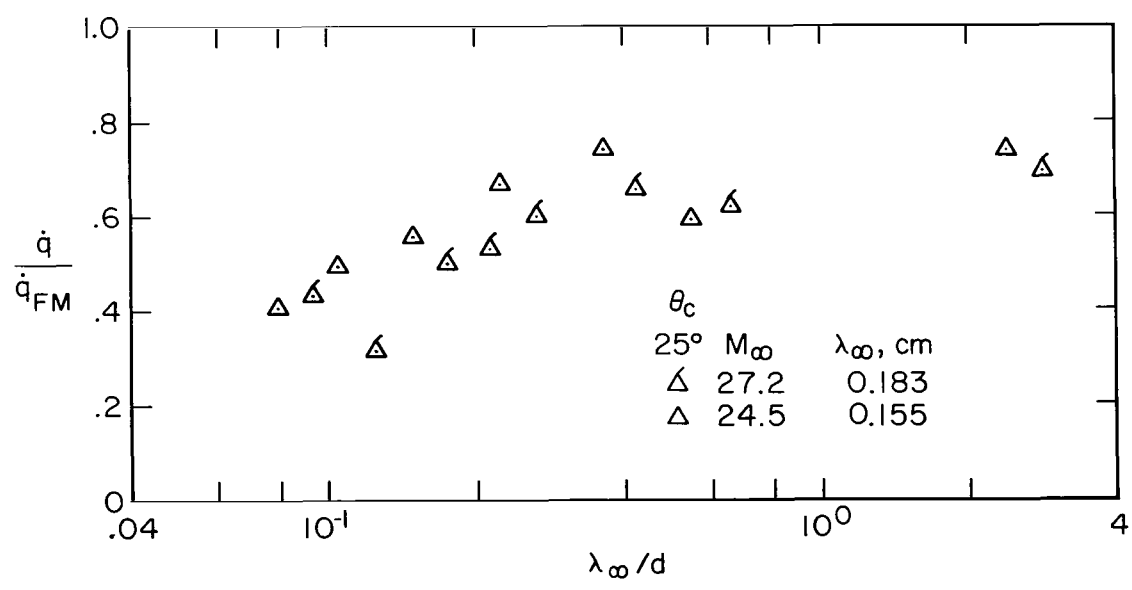


(a) $\theta_c = 3^\circ$

Figure 7.- Normalized heat-transfer coefficient variation with Knudsen number.



(b) $\theta_c = 10^\circ$



(c) $\theta_c = 25^\circ$

Figure 7.- Concluded.

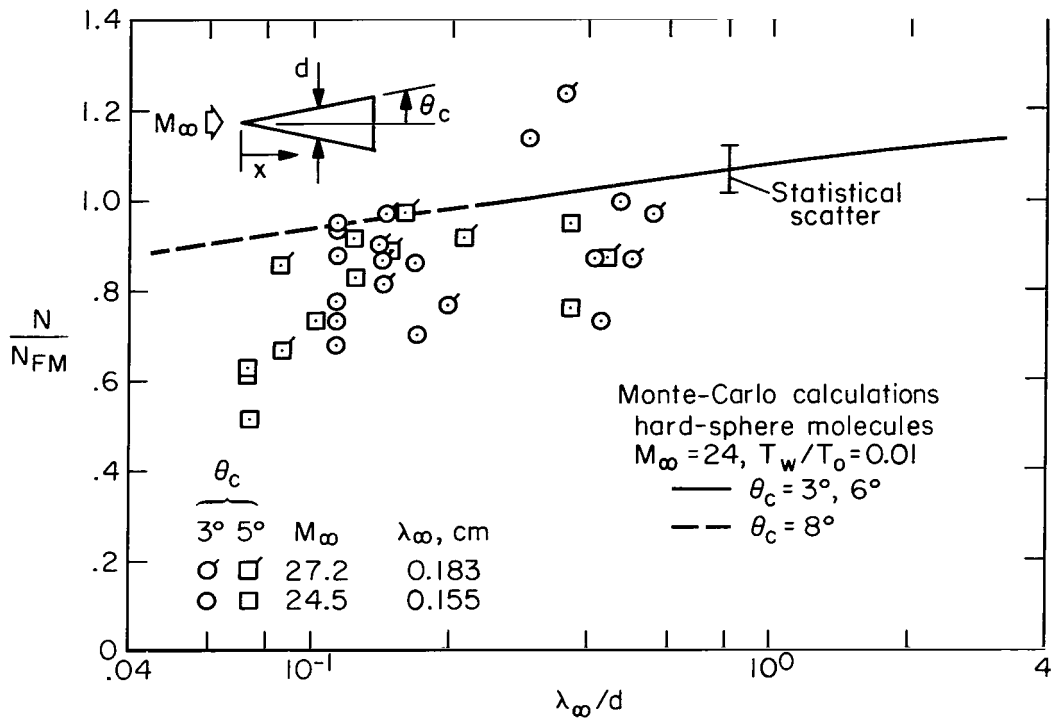


Figure 8.- Normalized number flux distribution on 3° and 5° half-angle cones.

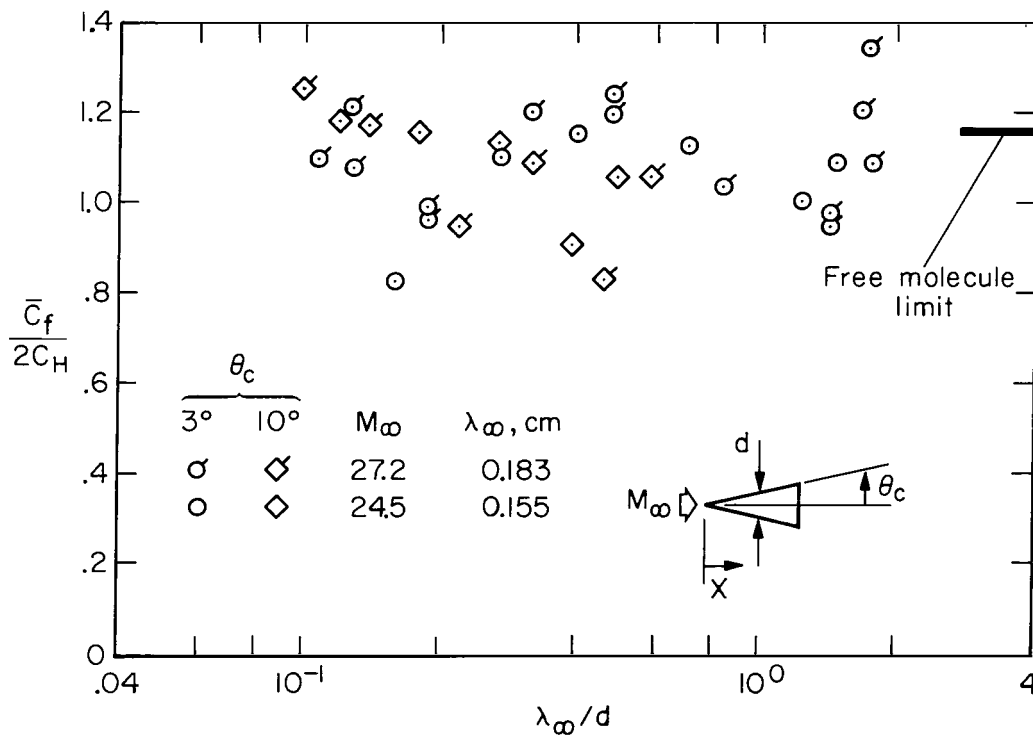


Figure 9.- Reynolds analogy factor for slender cones.



015 001 C1 U 12 720211 S00903DS
DEPT OF THE AIR FORCE
AF WEAPONS LAB (AFSC)
TECH LIBRARY/WLOL/
ATTN: E LOU BOWMAN, CHIEF
KIRTLAND AFB NM 87117

POSTMASTER: If Undeliverable (Section 158
Postal Manual) Do Not Return

"The aeronautical and space activities of the United States shall be conducted so as to contribute . . . to the expansion of human knowledge of phenomena in the atmosphere and space. The Administration shall provide for the widest practicable and appropriate dissemination of information concerning its activities and the results thereof."

— NATIONAL AERONAUTICS AND SPACE ACT OF 1958

NASA SCIENTIFIC AND TECHNICAL PUBLICATIONS

TECHNICAL REPORTS: Scientific and technical information considered important, complete, and a lasting contribution to existing knowledge.

TECHNICAL NOTES: Information less broad in scope but nevertheless of importance as a contribution to existing knowledge.

TECHNICAL MEMORANDUMS: Information receiving limited distribution because of preliminary data, security classification, or other reasons.

CONTRACTOR REPORTS: Scientific and technical information generated under a NASA contract or grant and considered an important contribution to existing knowledge.

TECHNICAL TRANSLATIONS: Information published in a foreign language considered to merit NASA distribution in English.

SPECIAL PUBLICATIONS: Information derived from or of value to NASA activities. Publications include conference proceedings, monographs, data compilations, handbooks, sourcebooks, and special bibliographies.

TECHNOLOGY UTILIZATION PUBLICATIONS: Information on technology used by NASA that may be of particular interest in commercial and other non-aerospace applications. Publications include Tech Briefs, Technology Utilization Reports and Technology Surveys.

Details on the availability of these publications may be obtained from:

SCIENTIFIC AND TECHNICAL INFORMATION OFFICE

NATIONAL AERONAUTICS AND SPACE ADMINISTRATION

Washington, D.C. 20546